Clay Minerals (2020), **55**, 293–302
doi:10.1180/clm.2020.40

CAMBRIDGE UNIVERSITY PRESS

Article

Structural transformation of kaolin as an active matrix for the *in situ* synthesis of zeolite Y

Jessyka Padilla[1]*, Alexander Guzman[2], Daniel Molina V[1] and Juan Carlos Poveda-Jaramillo[1]

[1]Universidad Industrial de Santander, Carrera 27 calle 9 Bucaramanga, Colombia and [2]ECOPETROL S.A. Instituto Colombiano del Petróleo, Piedecuesta, Colombia

Abstract

To produce an optimized matrix for the *in situ* crystallization of zeolite Y, a commercial kaolin chemically treated with NaOH solution at 97°C for 24 h and thermally transformed from 750 to 1100°C was studied. The kaolin calcined at 750°C has 20% more reactive tetrahedral aluminium species for the synthesis of zeolite Y than kaolin calcined at 865°C. The kaolin calcined at 1000°C has amorphous silica zones that may be extracted using caustic solution; this increases the surface area by a factor of 16 and generates mesopores ~5 nm in diameter. These structural changes in the calcined and treated kaolins were combined to prepare microspheres of the mesoporous matrix, upon which well-dispersed crystals of zeolite Y crystallized.

Keywords: FCC matrix, *in situ* hydrothermal synthesis, kaolin, phase transformation, zeolite NaY

(Received 10 August 2020; revised 14 December 2020; Accepted Manuscript online: 23 December 2020; Associate Editor: A. Turkmenoglu)

Introduction

Fluid catalytic cracking (FCC) is an important petroleum refining process, which produces most of the world's gasoline and a diesel precursor fraction. The catalyst used in the process consists of microspheres 40–100 μm in diameter, generally based on an ultra-stable zeolite Y and one or more components in the functional matrix (silica, alumina or amorphous silica-alumina), kaolin and a binder (Woltermann *et al.*, 1993). The industrial manufacture of the FCC catalyst can be carried out by incorporation or *in situ* routes (Woltermann *et al.*, 1993; Clough *et al.*, 2017). The *in situ* route offers greater benefits than incorporation because the zeolite grows directly on the pre-formed matrix microspheres, avoiding the use of a binder during the preparation of the catalyst and, moreover, improving zeolite dispersion. This favours the contact of reactants with the zeolite surface.

Traditionally, improvements in the performance of the FCC catalyst have focused on zeolites, but the properties of both the zeolite and the matrix should be combined to ensure efficient performance during catalytic cracking. In particular, the zeolite should be stabilized by the FCC matrix because this matrix is an attrition-resistant material, with high tolerance of metals and which improves the cracking of bottoms or bulky molecules such as those found in heavy vacuum gas oils (Magee & Mitchell, 1993). The *in situ* production of the FCC catalyst requires the formation of matrix composites prior to zeolite synthesis; consequently, kaolin clay has been used as a raw material to prepare microspherical composites due to its low cost and ready availability (Liu *et al.*, 2007; Zhang & Xiong, 2012a; Li *et al.*, 2017).

Kaolin is a clay rich in kaolinite, with minor impurities such as quartz, feldspars or micas. Kaolinite is a 1:1 layered aluminosilicate with a tetrahedral Si-sheet bonded to an octahedral aluminium (Al^{VI}) sheet (Massiot, 1995; Han *et al.*, 2016). Considering that kaolinite is the main component of kaolin, structural changes in this component will control zeolite crystallization. Depending on the thermal structural transformation of kaolin, the reactivity of this material can be modified by thermal treatment that may lead to more reactive SiO_2 or tetrahedral aluminium (Al^{IV}) species (Lee *et al.*, 1999; Wang *et al.*, 2011; Liu *et al.*, 2015). Specifically, between 450°C and 900°C, the formation of the metakaolin phase is driven by dehydroxylation which distorts the crystalline structure by the migration of Al atoms to vacant sites in the interlayer, resulting in a change of the Al coordination from octahedral to tetrahedral (Sperinck *et al.*, 2011; Li *et al.*, 2017). Also, during calcination at the temperature of the exothermic reaction at ~980°C, the kaolin is transformed into an Al-Si spinel or gamma-alumina with reactive SiO_2 species (Chakravorty *et al.*, 1986).

Furthermore, during thermal transformation over 500°C, the tetrahedral sheets are also disrupted, increasing the amount of soluble silica, which in solution may form polymeric species and nuclei of aluminosilicate (Madani *et al.*, 1990). Specifically, at temperatures of 600–800°C, the metakaolin is vulnerable to alkali attack, releasing $Al(OH)_4$ and SiO_4^{4-} species in solution (Madani *et al.*, 1990; Johnson & Arshad, 2014). Therefore, the formation of metakaolin from kaolinite is an activation process, where the structure reaches a metastable amorphous and highly reactive phase that may transform to zeolite (Feng *et al.*, 2009).

Thus, kaolin activation temperatures are important to determine the optimal conditions for crystallization of zeolite Y. It is also challenging to obtain the correct formulation of a thermally pre-treated kaolin mixture to be used as a microspherical matrix to manufacture of FCC catalysts *in situ*. This matrix should be reactive and sufficiently strong to maintain its morphology before and after the synthesis of zeolite Y.

In the 1960s, zeolite Y was implemented in the FCC process; since then, several modifications to the catalyst have been

*E-mail: jessyka.padilla@correo.uis.edu.co, jessykpadilla@hotmail.com

Cite this article: Padilla J, Guzman A, Molina D, Poveda-Jaramillo JC (2020). Structural transformation of kaolin as an active matrix for the *in situ* synthesis of zeolite Y. *Clay Minerals* **55**, 293–302. https://doi.org/10.1180/clm.2020.40

developed to improve its performance (Sadeghbeigi, 2012). These improvements were based on alumina-rich matrices for nickel passivation (Salagre *et al.*, 1996; Feng *et al.*, 2014), vanadium traps (Lin *et al.*, 1997), ion-exchange of the zeolite with rare earth metals to improve its stabilization and conversion (Sousa-Aguiar *et al.*, 2013) and the use of additives for specific purposes (Andersson *et al.*, 1999; Degnan *et al.*, 2000). Since the 1980s, FCC processing of the resid feed has boomed, leading efforts towards improving the porosity of the FCC catalyst for the conversion of these feedstocks. This purpose has been achieved by using the ultrastable zeolite Y; however, regarding the matrix, Engelhard corporation (now acquired by BASF) introduced DMS (Distributed Matrix Structures) technology with high acceptance in refineries around the world. (Pan *et al.*, 2015; Clough *et al.*, 2017). The pore architecture of matrix-DMS contains a substantial void volume and macroporous surface area designed to facilitate the diffusion of reagents and products, reduce over-cracking (short contact times) and coke selectivity.

Despite the fact that FCC is a mature process, the oil industry continuously requires specific advances and improvements for additives and catalysts according to their daily challenges in the FCC-units. Therefore, in this work, a commercial kaolin was investigated as a matrix for obtaining FCC catalysts. With this purpose, the kaolin was thermally treated at temperatures of 750, 865, 950, 980, 1000, 1030, 1050 and 1100°C. In addition, the calcined samples were reacted with a caustic solution at 97°C for 24 h to increase their specific surface areas by modifying their crystal order and structures, mediated by leaching Si and Al from kaolin to the alkaline solution. Thus, by combining thermal and chemical treatment of kaolin, materials with better textural properties and greater porosities may be obtained that can be used to produce more efficient and selective FCC catalysts with improved diffusion properties for larger hydrocarbon molecules.

Experimental

Kaolin

The kaolin (K) was obtained from Caolines de Vimianzo, Italy; its mineralogical composition is kaolinite (88.0 mass%), muscovite $2M_1$ (8.6 mass%) and quartz (3.4 mass%). The kaolinite had a low Hinckley index (0.52) determined by X-ray powder diffraction (XRD).

Calcination of kaolin

The kaolin was calcined in a Nabertherm oven at 750, 865, 980, 1000, 1030, 1050 and 1100°C for 1 h with a heating rate of 5°C/min. These samples were denoted as K-T, where T refers to the calcination temperature.

Alkaline treatment

Sodium hydroxide (NaOH, Merck) was used as alkaline reagent to prepare the K-TA samples (where A indicates alkaline treatment). The reactivity and leaching (Si, Al) of the K-T samples were measured with a 3.5 M aqueous NaOH solution (5 g per gram of calcined kaolin) refluxed at 97°C for 24 h.

Matrix preparation

An aqueous kaolin slurry, 40 mass% and a mass ratio 1:1.5:0.16 of kaolin:water:sodium silicate solution, was prepared. 8 g of sodium silicate solution (28.5 mass% SiO_2, 8.5 mass% Na_2O; Merck) and 75 g of deionized water were mixed with an ULTRA-TURRAX T 50 Pilot Scale disperser/homogenizer at 4000 rpm, for 5 min. Then, 50 g of the kaolin powder (25 g of raw, 7.5 g calcined and 17.5 g of alkaline treated kaolin) were added and mixed for 15 min. Matrix microspheres were obtained by spray drying with a flow of 3 mL/min and adjusting the inlet temperature to 135–140°C at an air pressure 0.59 MPa, atomization air flow of 8–10 L/min and dried air flow of 70 L/min. The microspheres obtained were sieved between 40 and 90 μm and calcined in a muffle oven at 750°C for 3 h.

In situ synthesis of NaY

In situ growth of the zeolite NaY on the matrix was carried out by hydrothermal synthesis. The reaction gel was prepared with sodium silicate solution, microspheres and seeds with a molar ratio of $1.9Na_2O : 5.1SiO_2 : Al_2O_3 : 74.1H_2O$. A seed solution was prepared according to the stereochemistry reported by Qiang *et al.* (2010) and was aged at 22°C for 6 h. Hydrothermal crystallization was carried out in Teflon reactors with a stainless-steel cover at 100°C for 24 h. The solid product was separated by filtration, washed thoroughly with deionized water, and dried for 12 h at 90°C.

The H-form of the sample was obtained by ion exchange using an aqueous solution at 15 mass% of NH_4NO_3 (≤100%; Merck) at 85°C for 1 h under stirring at 50 rpm. After the exchange step, the sample was washed and dried. The NH_4-Y sample on the matrix was calcined at 600°C.

Characterization techniques

Differential scanning calorimetry and thermogravimetric (TG-DSC) analysis was conducted on a Mettler Toledo TGA/DSC 3+ instrument. The sample was placed in a platinum crucible and heated at a rate of 5°C/min from room temperature to 1100°C using N_2 as a carrier gas. The mineralogy of the end products was determined by X-ray diffraction (XRD). The XRD traces were collected in a RIGAKU Smartlab SE Advance powder diffractometer, using Cu-*Kα* radiation operating at 50 kV and 40 mA. The kaolin samples and NaY/matrix were collected with scanning step at 0.2°2θ (5.0°2θ/min) and 0.015°2θ (1.2°2θ/min), respectively.

The textural properties of calcined and alkaline treated kaolins were determined by nitrogen adsorption at −196°C in a Micromeritics ASAP 2020 automated analyzer, after sample degassing at 350°C under vacuum. The acidity of the samples was determined by temperature-programmed desorption of ammonia (NH_3-TPD) using a Micromeritics AutoChem II apparatus equipped with a thermal conductivity detector. Approximately 0.5 g of the sample was charged in the quartz tube and heated at 10°C/min to 550°C for 1 h under a He flow, before saturation with NH_3 at 100°C for 30 min. The NH_3-TPD profile was recorded from 100 to 550°C. The raw kaolin alone was heated to 350°C for degassing and the TPD test.

The samples were digested in a microwave oven for determination of bulk elemental composition. The solutions obtained were analyzed by inductively coupled plasma atomic emission spectroscopy (ICP-OES) using an Optima 8300 system and external standardization. The morphological analysis of the NaY/Matrix was analyzed with a QUANTA 450 a LEO 1450 VP electron microscopes equipped with OXFORD scattered energy X-ray systems operated in the high vacuum and low vacuum modes.

https://doi.org/10.1180/clm.2020.40 Published online by Cambridge University Press

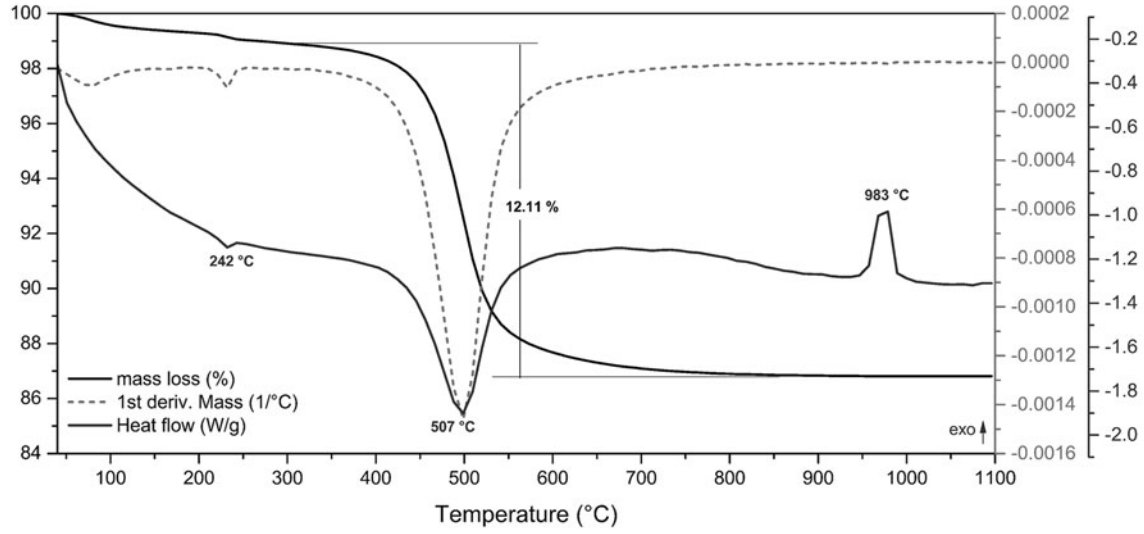

Fig. 1. TG-DSC curves of kaolin.

The images were obtained using a backscattered electron detector (BSE).

Solid State Nuclear Magnetic Resonance (ssNMR) spectra of kaolin powders were collected in a Bruker Avance wide bore spectrometer operating at 9.4 T. Samples were packed in 4 mm zirconia rotors and measured by spinning at 10 kHz under Magic Angle Spinning (MAS) condition at 298 K. The ^{27}Al-ssNMR experiments were carried out using 104.24 MHz as

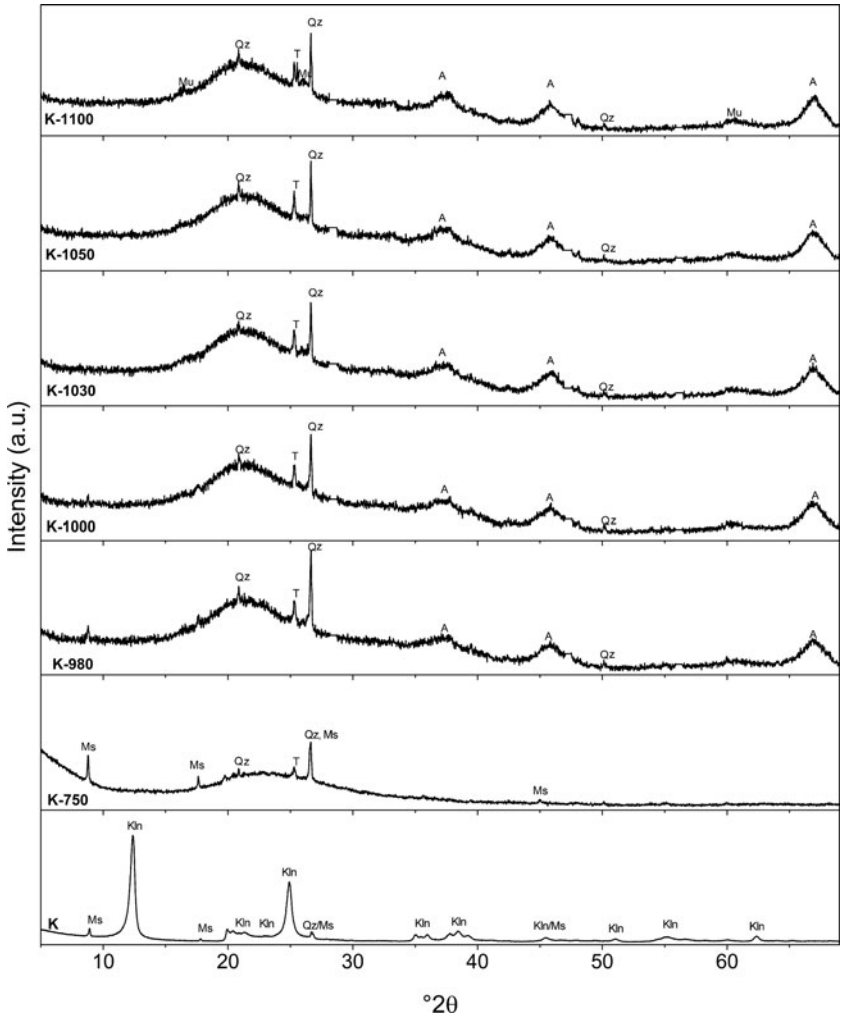

Fig. 2. XRD traces of the original kaolin and the kaolin calcined at 750, 980, 1000, 1030, 1050 and 1100°C. Kln: Kaolinite, Qz: Quartz, Ms: Muscovite, T: Titanium dioxide, A: γ-Alumina or Al-Si spinel, Mu: Mullite.

https://doi.org/10.1180/clm.2020.40 Published online by Cambridge University Press

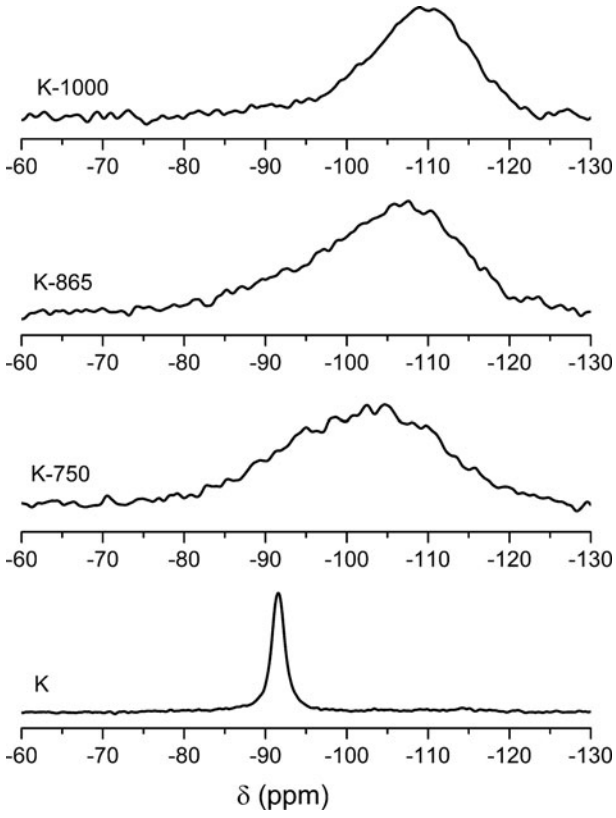

Fig. 3. ^{29}Si-MAS NMR spectra of K and calcined kaolin at 750, 865 and 1000°C.

the resonance frequency and a modified zgig pulse program to obtain a flip angle of π/12, spectral window of 52.6 kHz (500 ppm), time domain 2626 points, acquisition time of 24.9 ms, proton decoupling during acquisition, 4096 scans and 1.0 of recovery time. For ^{29}Si-ssNMR experiments the resonance frequency was 79.48 MHz and a zgig pulse program was used with a flip angle of π/6, spectral window of 23.8 kHz (299.6 ppm), time domain 4096 points, acquisition time 86.0 ms, proton decoupling during acquisition, 1024 scans, and 50s of recovery time.

Results and discussion

Calcined kaolin

The calcination temperatures of kaolin were chosen according to the result of TG-DSC analysis (Fig. 1). The formation of metakaolin is associated with a mass loss of 12.1 mass% between 350 and 800°C in TGA, and the endothermic band of the DSC signal centered at 507°C corresponds to the dehydroxylation of kaolinite layers (Kumar *et al.*, 2013; Ptáček *et al.*, 2014). The transformation to Al-Si spinel or gamma-alumina phase is confirmed by the exothermic peak at 983°C for this kaolin sample (Lee *et al.*, 1999; Wang *et al.*, 2011). The structural changes of kaolin after calcination were analyzed according to the XRD traces (Fig. 2). The original sample (K) exhibits a characteristic diffraction profile of poorly crystalline kaolinite ($I_H = 0.52$) and minor quantities of muscovite and quartz (Plançon *et al.*, 1988; Du *et al.*, 2010). The broad hump observed between 15 and 35°2θ on the XRD traces indicate the loss of crystalline ordering after dehydroxylation by heating at 750°C. This hump shifts towards lower angles with increasing calcination temperature, which is due to bonds

Table 1. Signal assignment of ^{29}Si NMR in calcined kaolin.

Sample	K-750	K-865	K-1000
Signal assignment		δ-^{29}Si (ppm)	
Q^4 Si(0Al)	−104; −109; −116	−106; −110; −117	−105; −108; −111; −115; −119
Q^4 Si(1Al) Q^3 [$(SiO)_3SiOH$]	−99; −101	−99; −102	−101
Q^4 Si(2Al) Q^3 [$(SiO)_2(AlO)SiOH$] Q^2 [$(SiO)_2Si(OH)_2$]	−94	−92; −95	−90, −94
Q^4 Si(3Al) Q^3 [$(SiO)(AlO)_2SiOH$] Q^2 [$(AlO)_2Si(OH)_2$] Q^2 [$(SiO)(AlO)Si(OH)_2$]	−83; −89	−86; −89	–

breaking between the tetrahedral sheet and octahedral sheet producing amorphous silica (Lee *et al.*, 1999). The Si-Al spinel phase, also referred to as γ-alumina, is formed near the exothermic event of kaolinite and appears in the XRD trace of K-980 and persists in sample K-1100 (Leonard, 1977; Chakravorty *et al.*, 1986; Low & McPherson, 1988). After calcination at ∼1050°C, the spinel begins its structural transformation to the inert mullite phase that provides attrition resistance to the catalyst. Mullite was detected in the XRD trace of sample K-1100 (Zheng *et al.*, 2005a; Zhang & Xiong, 2012a).

The ^{29}Si-MAS NMR spectrum of raw kaolin exhibited a resonance of ^{29}Si at δ = −91.5 ppm, assigned as a Q^3 site in silicate sheets, where each SiO_4 tetrahedron shares three apices with another SiO_4 unit (Fig. 3) (Mägi *et al.*, 1984). After calcination, the endothermic loss of OH groups causes a complex amorphous structure with formula $Al_2Si_2O_7$ consisting of a random mixture of amorphous SiO_2 and Al_2O_3 units that still retains a low degree of crystalline order in hexagonal sheets (Zhang & Xiong, 2012a). Therefore, the ^{29}Si-MAS NMR spectra of the calcined samples were not smoothed because of the different chemical environments of silicon as Q^4 [(SiO) 4Si], Q^3 [$(SiO)_3SiOH$] species. Finally, Q^2 [$(SiO)_2Si(OH)_2$] and Q^1 [$(SiO)Si(OH)_3$] sites characteristic of silicates, include Q^4 units in Si (nAl) with tetrahedral aluminium (Al^{IV}) in the second coordination sphere, where n = 0–4 (Table 1) (Man *et al.*, 1990; Mackenzie & Smith, 2013). Moreover, as the calcination temperature increased, an up-field shift of the maximum of ^{29}Si NMR signal occurred, specifically with Q^4 (1Al) and Q^3 (2Al) species at 750°C and Q^4 (0Al) at 1000°C, which is related to the formation of amorphous SiO_2 as was revealed in the XRD trace of sample K-1000 (Rocha & Klinowski, 1990).

The ^{27}Al-MAS NMR spectrum of the hydrated kaolin shows a resonance of ^{27}Al at δ = 0 ppm corresponding to octahedral aluminium (Al^{VI}) in the gibbsite-like sheets of the kaolinite and muscovite phases (Fig. 4) (Massiot, 1995; Mackenzie & Smith, 2013). Besides, the structural changes in the calcined kaolins were also observed in the ^{27}Al-MAS NMR spectra (Fig. 4). In the metakaolin phase, an increase in 4- and 5-coordinated Al species was observed, where K-750 shows more Al^{IV} compared with K-865, which might be active in the synthesis of zeolite Y. In contrast, sample K-1000 in the Al-Si spinel phase increases the proportion of Al^{VI}.

Alkaline reaction

During the alkaline reaction of the samples under hydrothermal conditions, leaching of the soluble Si species and changes in the

https://doi.org/10.1180/clm.2020.40 Published online by Cambridge University Press

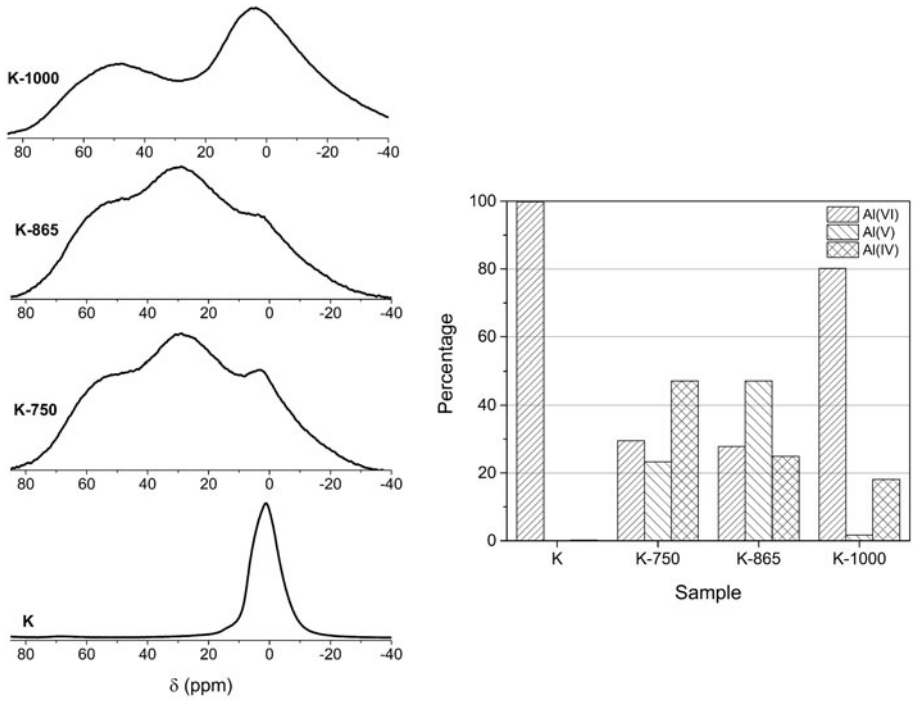

Fig. 4. ^{27}Al-MAS NMR spectra of K and calcined kaolin at 750, 865 and 1000°C.

Table 2. Textural properties and NH_3-TPD of kaolin samples.

Sample	S_{BET} (m^2/g)	S_{Micro} (m^2/g)	S_{Ext} (m^2/g)	V_p (cm^3/g)[a]	Acidity (μmol_{NH3}/g)
K	17	9	8	0.12	0
K-750	19	4	15	0.12	40.7
K-865	15	6	9	0.12	41.5
K-980	9	4	5	0.09	16.8
K-1000	9	6	3	0.09	21.5
K-1030	8	8	0	0.10	13.9
K-1050	8	5	2	0.10	16.0
K-1100	6	6	1	0.08	11.7
K-A	26	12	14	0.12	0
K-750A	4	4	0	0.01	1723.1
K-865A	5	5	0	0.02	1487.9
K-980A	163	15	147	0.36	222.0
K-1000A	171	22	149	0.34	228.3
K-1030A	167	16	151	0.33	215.8
K-1050A	207	13	194	0.44	210.1
K-1100A	169	1	168	0.35	181.0

[a]V_p at $P/P_0 \approx 1.0$.

textural properties with respect to the calcined kaolins without alkaline treatment occur (Table 2). The raw kaolin did not present any significant change in textural properties after the alkaline reaction (Fig. 5). However, samples calcined at temperatures >980°C reacted with $NaOH_{(ac)}$ formed a mixture of amorphous SiO_2-Al_2O_3-species with a new external surface area and a larger pore size and total pore volume (Table 2). Also, the starting kaolin had a type III isotherm characteristic of non-porous materials, which was transformed after alkaline treatment into a type VI isotherm with steps, indicating multiple pore sizes (Rouquerol *et al.*, 1998; Condon, 2006). The kaolins calcined at >980°C and treated with alkali kaolins showed a substantial increase in mesopores of ~5 nm diameter (Fig. 5), which would facilitate the diffusion of bulky molecules in the FCC matrix prepared with them.

In contrast, the metakaolin samples calcined at 750 and 865°C were reactive under alkaline reaction conditions, resulting in the successful formation of zeolite NaA (Fig. 6), $Na_{12}(Al_{12}Si_{12}O_{48})\cdot nH_2O$, with Si/Al = 1, like kaolinite. This was also confirmed by the type I isotherm characteristic of microporous materials (Fig. 5) and the high acidity value determined by NH_3-TPD (Table 2). The ammonia desorption thermograms allow identification of the distribution of the acid sites strength of the material analysed. In this manner, although the calcined kaolins have a small number of acid sites accessible to ammonia (Table 2), these sites also have very weak acidity because their maximum desorption appears at ~130°C for all samples (Fig. 7). Nevertheless, samples subjected to alkaline treatment did not show an increase in total acidity. In particular, samples K-750A and K-865A show two maxima on the TPD graph. However, although K-865A has lower total acidity, it has stronger acidic sites compared to K-750A.

The kaolin serves as a support for the zeolite Y during *in situ* synthesis. However, being an alumino-silicate material itself, it also provides the sources required for crystallization, avoiding the use of binders for the zeolite and the matrix. Specifically, the fully calcined kaolin (≥1000°C) acts as a source of Si. The formation of the Si-Al spinel phase in kaolin K is marked by the exothermic signal at 983°C and is usually referred to as γ-Al_2O_3, due to its similar structure (Figs 1–2). The γ-Al_2O_3 phase has tetragonal symmetry with $a = 0.7906$ nm and $c/a = 0.985$, while the Si-Al spinel obtained has cubic symmetry with $a = 0.7886$ nm, because of the smaller ionic radius of Si^{4+} occupying positions of Al^{3+} (Sonuparlak *et al.*, 1987; Low & McPherson, 1988). Due to its poor crystal order, it was difficult to determine an exact structure of the Si-Al spinel in K-1000 (Fig. 2). However, it was observed in the ^{29}Si-NMR spectra that this sample is also rich in Q^4 (0Al) silicon environments (Fig. 3), which indicates a secondary amorphous SiO_2 phase after the thermal treatment of kaolin (Lee *et al.*, 1999). This amorphous SiO_2 had been referred to as active silica for the synthesis of zeolites, but its presence in K samples calcined at temperatures above 980°C may also be associated

https://doi.org/10.1180/clm.2020.40 Published online by Cambridge University Press

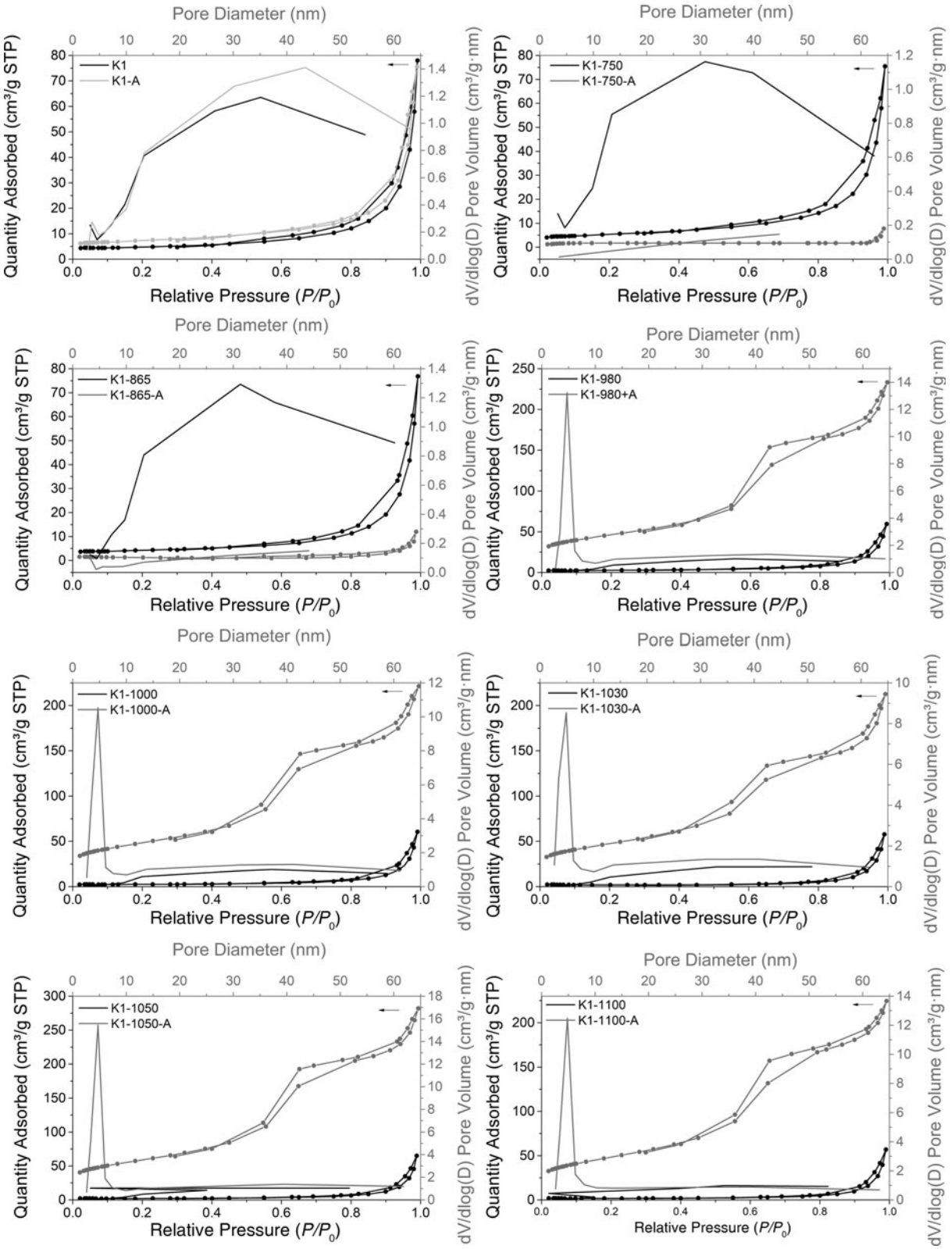

Fig. 5. Nitrogen adsorption/desorption isotherms and differential pore-size distributions for the thermal (black) and alkali treatment (grey) samples.

with the hump between 20 and 25°2θ (Fig. 2). A matrix highly enriched in spinel was used by Guo *et al.* (2011) to obtain the zeolite L, because this matrix exhibits significant tolerance to heavy-metals, improving the catalyst life.

The amount of the amorphous SiO_2 in calcined kaolins may be expressed by alkaline solubility using a NaOH solution (Okada *et al.*, 1986; Sonuparlak *et al.*, 1987; Zheng *et al.*, 2005b). However, in the present study, the extraction of Si species from

https://doi.org/10.1180/clm.2020.40 Published online by Cambridge University Press

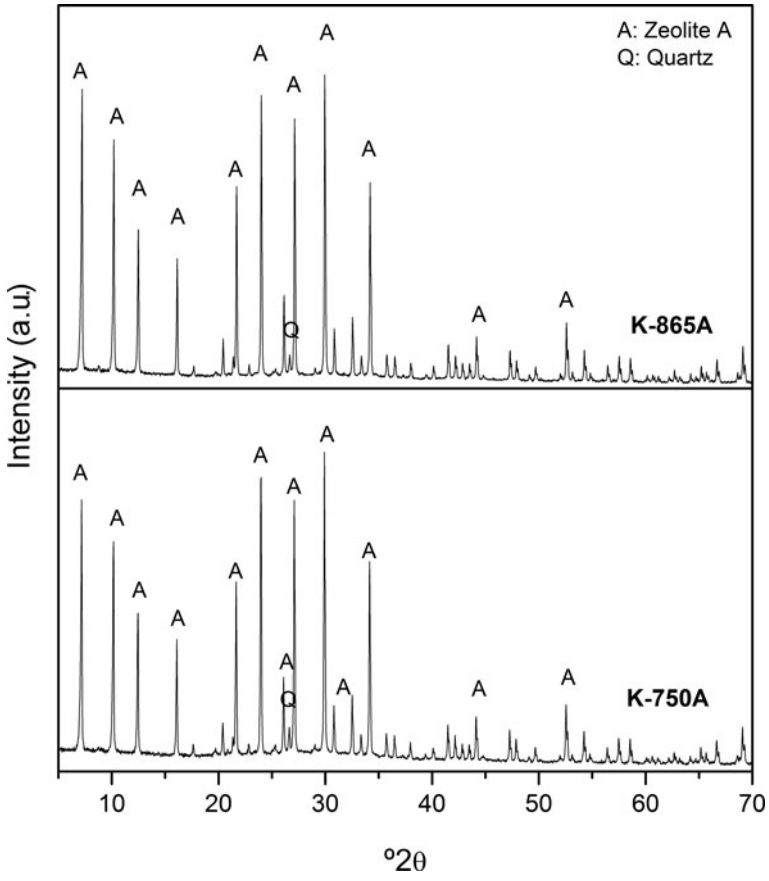

Fig. 6. XRD traces of zeolite A crystallized during alkaline treatment of K-750 and K-865.

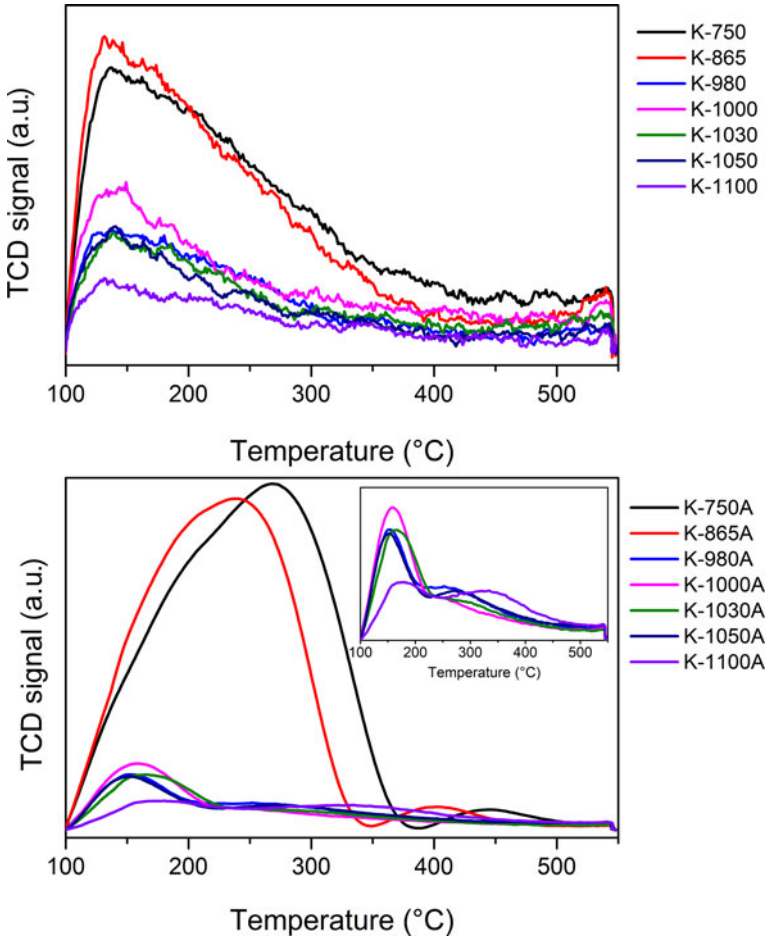

Fig. 7. Ammonia-TPD plots of calcined kaolins (upper) and with alkaline treatment (lower).

https://doi.org/10.1180/clm.2020.40 Published online by Cambridge University Press

Table 3. Textural properties of matrix and NaY/matrix.

Sample	S_{BET} (m^2/g)	S_{Micro} (m^2/g)	V_p (cm^3/g)[a]	V_{micro} (cm^3/g)	V_{meso} (cm^3/g)[b]	Si/Al[c]	Acidity[d] (μmol $_{NH3}$/g)
Matrix	31	3	0.10	–	0.10	0.88	52.2
NaY/matrix	276	224	0.23	0.09	0.13	1.14	447.7

[a]V_p at $P/P_0 \approx 1.0$.
[b]BJH Adsorption cumulative volume of pores.
[c]ICP-OES.
[d]After ion-exchange with NH_4NO_3.

fully calcined samples favours the increase in the external surface area and the pore volume. This leads to a matrix rich in Al_2O_3, which in turn shows greater acidity (Fig. 5, Table 2). The normalized mass desorption of ammonia showed a change in the distribution of the acid strength of chemically treated kaolins (Fig. 7). For instance, the K-980A, K-1000A, K-1030A, and K-1050A samples exhibited two desorption maxima close to 170 and 270°C, indicating a 10-fold increase in weak acid sites compared to the kaolins with only thermal treatment. By contrast, the K-1100A sample showed an increase and shift of the second TPD-peak towards 340°C, indicating the presence of sites of medium acidity. These weak to medium acid sites are characteristic of amorphous SiO_2-Al_2O_3 species, where the strongest sites are related more to a small amount of substituted aluminium in the silica network forming Brønsted acid sites, while the weakest are usually provided by Al_2O_3 agglomerates associated with Lewis sites or their interaction with silanol or aluminol groups (Hensen *et al.*, 2012).

On the other hand, metakaolin is produced after decomposition of the kaolinite structure by a dehydroxylation reaction, which starts at ~400°C and is characterized by an amorphous structure but retains the tetrahedral sheets up to 920°C (Lee *et al.*, 1999). The loss of OH-groups produces a partially-disordered structure accompanied by a mass loss and vanishing reflections of kaolinite in the XRD traces (Fig. 1–2). This mainly affects the octahedral sheet, as was observed in the ^{27}Al-NMR spectra (Fig. 4) (Massiot, 1995; Zheng *et al.*, 2005b). After calcination, 47% of the octahedral Al was converted to Al^{IV} in sample K-750, while, in K-865, only 25% of Al^{IV} was obtained. Thus, K-750 was used as an Al source for the synthesis of zeolite Y because it contained most Al^{IV}. Unlike kaolin calcined at temperatures ≥980°C, the metakaolin samples reacted to form type A zeolite when treated with alkali solution (Fig. 6). This crystallization of Linde type A zeolite from metakaolin was reported in previous studies (Heller-Kallai & Lapides, 2007; Ayele *et al.*, 2016; Pereira *et al.*, 2018). The formation of zeolite A occurs as

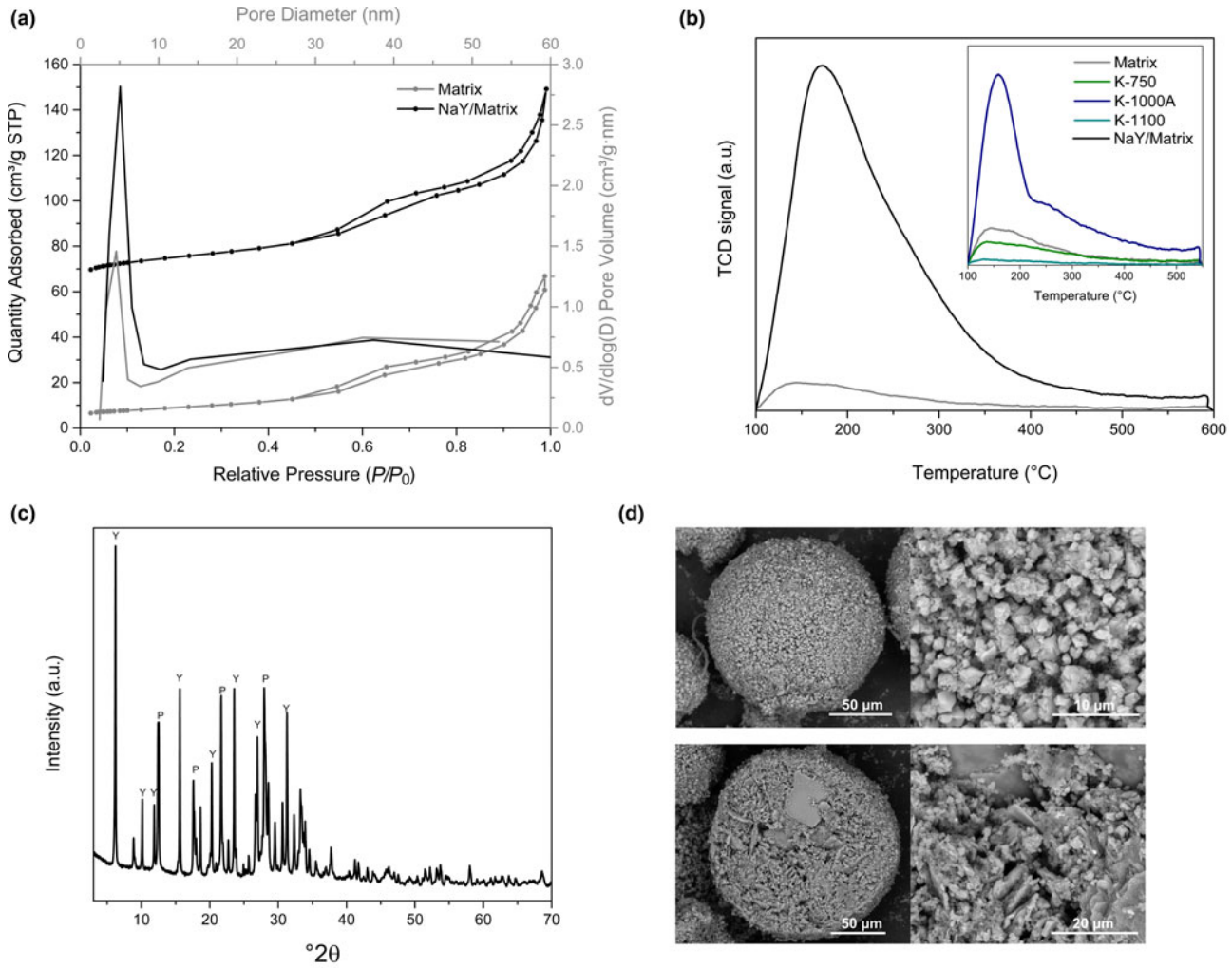

Fig. 8. (a) Nitrogen adsorption/desorption isotherms and differential pore-size distributions, (b) Ammonia-TPD plot of matrix (grey) and NaY/matrix (black), (c) XRD trace and (d) SEM imagens of NaY/matrix.

https://doi.org/10.1180/clm.2020.40 Published online by Cambridge University Press

a product of the re-precipitation of $H_2SiO_4^{2-}$ and $Al(OH)_4^-$ species dissolved from the metakaolin in contact with the alkaline solution (Peng *et al.*, 2018). Likewise, the prominent increase in the acidity of samples K-750A and K-865A is related to the low Si/Al ratio in zeolite A; the large amounts of structural Al increases the density of acid sites in the region between 200 and 300°C in those samples, as shown in the TPD graph (Fig. 7).

In situ crystallization of NaY

The *in situ* synthesis of zeolite Y from kaolin has been reported using a mixture of metakaolin microspheres calcined at 700°C and/or kaolin microspheres calcined at 1000°C (Xu *et al.*, 2000; Patrylak *et al.*, 2001; Wei *et al.*, 2010; Zhang & Xiong, 2012a; Zheng *et al.*, 2015). In this work, instead of making a mixture of calcined microspheres, homogeneous particles were prepared using proportions based on the analysis of thermally and chemically treated kaolin. Thus, matrix microspheres were obtained with an aqueous slurry composed of a 50:35:15 mass percentage mixture of K, K-1000A and K-1100 samples. After spray drying, the particles were calcined to transform the hydrated kaolin fraction into metakaolin. As mentioned previously, 750°C was chosen as the calcination temperature due to greater contents of Al^{IV} (Fig. 4), which could provide sites for the formation of zeolite Y. Even though sample K-1050A shows a greater surface area and total pore volume (Table 2), it is known that at this temperature the spinel phase begins its transformation to inert components, such as mullite and cristobalite, which would not have reactive amorphous SiO_2 during *in situ* crystallization (Rocha & Klinowski, 1990; Zhang & Xiong, 2012b; Liu *et al.*, 2015). Meanwhile, K-1100 was added to the matrix to provide mechanical resistance to the particle (Zheng *et al.*, 2005a).

The matrix displayed a BET specific surface area of 31 m^2/g and 52.2 $\mu mol_{NH3}/g$ (Table 3), although a greater specific surface area and acidity was anticipated. This might be attributed to the sodium silicate added to the slurry as a dispersant forming another dense phase with the components during spray drying. Nevertheless, during *in situ* hydrothermal crystallization, the active species of Si and Al present in the matrix were dissolved in alkaline pH forming a supersaturated solution on the surface of the microspheres to favor the growth of zeolite Y (Liu *et al.*, 2003). In this process of dissolution of the active species from the matrix, the volume of mesopores between 3 and 10 nm (Fig. 8a) increased by ~30% after synthesis of NaY (Table 3). Likewise, the NaY/matrix exhibited a type IV nitrogen adsorption-desorption isotherm with a higher hysteresis loop compared to the matrix, indicating a higher content of mesopores produced by alkaline leaching. Furthermore, the NH_3-TPD curve showed the strength distribution of the acid sites on the catalyst NaY/matrix (Fig. 8b). The samples were previously ion-exchanged with NH_4NO_3. After *in situ* synthesis, the maximum desorption was shifted towards higher temperatures, ~180°C, and a shoulder at >250°C was also observed, indicating that zeolite HY had a large number of mildly acidic sites.

The synthesis of the zeolite NaY on the matrix was confirmed by the XRD trace (Fig. 8c). Zeolite crystallinity in the samples was determined according to Zheng *et al.* (2005b) using as 100% a reference sample prepared with kaolin microspheres calcined at 750°C (metakaolin) following the same synthesis procedure as described above. The calculated relative crystallinity for the NaY zeolite/matrix was 98.6% (Zheng *et al.*, 2005b). Zeolite P was also identified as a secondary and undesired phase during *in situ* synthesis, which can be attributed to the fact that pure reagents and structure-directing agents are not used in this mode of synthesis (Lutz, 2014; Garcia *et al.*, 2018). According to the quantitative analysis of the X-ray diffraction profile of NaY/matrix, 69.0% of zeolite Y (PDF: 01-084-9686) and 21.3% of zeolite P (PDF: 01-080-0699) were obtained. In addition, SEM images of NaY/matrix support the XRD results (Fig. 8d). In these micrographs, pseudo-cubic zeolite crystallites are completely dispersed over and inside the surface of the matrix microspheres; interparticle voids between 120 nm to 3 μm were also observed. The arrangement of the zeolite, porosity properties and voids provide an improved performance for the catalyst as these morphological properties would reduce the occlusion of active sites and would favour the diffusivity of reagents and products.

Conclusions

The calcination of kaolin at 750°C provides a better active source of Al^{IV} for the growth of zeolite Y than does metakaolin obtained at 865°C. Kaolin calcined at temperatures above the exothermic point and treated with alkali increase the mesoporosity to sizes of 3–10 nm. The mixture of these properties of the calcined and modified kaolins was used to manufacture an active FCC matrix, and a well-crystallized zeolite NaY was synthesized.

This methodology for the preparation of cracking catalysts should be implemented to improve the diffusion of heavy feedstocks due to the system of mesopores and cavities with pore openings from 120 nm to 3 μm. In addition, a good dispersion of the zeolite on the surface of microspheres was obtained, which would favour the accessibility of the reactant molecules to active sites.

Financial support. The authors are grateful to Vicerrectoria de Investigación of Universidad Industrial de Santander (Colombia) and for the financial support of Colciencias-Ecopetrol Contract number 403-2013, Mining and Energy Program.

References

Andersson P.O.F., Pirjamali M., Järås S.G. & Boutonnet-Kizling M. (1999) Cracking catalyst additives for sulfur removal from FCC gasoline. *Catalysis Today*, **53**, 565–573.

Ayele L., Pérez-Pariente J., Chebude Y. & Díaz I. (2016) Conventional versus alkali fusion synthesis of zeolite A from low grade kaolin. *Applied Clay Science*, **132–133**, 485–490.

Chakravorty A.K., Ghosh D.K. & Kundu P. (1986) Structural characterization of the spinel phase in the kaolin–mullite reaction series through lattice energy. *Journal of the American Ceramic Society*, **66**, 610–612.

Clough M., Pope J.C., Tan L., Lin X., Komvokis V., Pan S.S. & Yilmaz B. (2017) Nanoporous materials forge a path forward to enable sustainable growth: Technology advancements in fluid catalytic cracking. *Microporous and Mesoporous Materials*, **254**, 45–58.

Condon J.B. (2006) *Surface Area and Porosity Determinations by Physisorption*. P. in.: 1st edition. Elsevier Science, Amsterdam, The Netherlands, 296 pp.

Degnan T.F., Chitnis G.K. & Schipper P.H. (2000) History of ZSM-5 fluid catalytic cracking additive development at Mobil. *Microporous and Mesoporous Materials*, **35–36** 245–252.

Du J., Morris G., Pushkarova R.A. & Smart R.S.C. (2010) Effect of surface structure of kaolinite on aggregation, settling rate, and bed density. *Langmuir*, **26**, 13227–13235.

Feng H., Li C. & Shan H. (2009) Effect of calcination temperature of kaolin microspheres on the in situ synthesis of ZSM-5. *Catalysis Letters*, **129**, 71–78.

https://doi.org/10.1180/clm.2020.40 Published online by Cambridge University Press

Feng R., Bai P., Liu S., Zhang P., Liu X., Yan Z., Zhang Z. & Gao X. (2014) The application of mesoporous alumina with rich Brönsted acidic sites in FCC catalysts. *Applied Petrochemical Research*, **4**, 367–372.

Garcia G., Cabrera S., Hedlund J. & Mouzon J. (2018) Selective synthesis of FAU-type zeolites. *Journal of Crystal Growth*, **489**, 36–41.

Guo S., Yu Z., Chen Y. & Chen X. (2011) In situ synthesis of zeolite NaKL in highly-enriched spinel matrix. Pp. 1045–1048 in: *Advanced Materials Research*. Trans Tech Publications, Zurich, Switzerland.

Han Y., Liu W. & Chen J. (2016) DFT simulation of the adsorption of sodium silicate species on kaolinite surfaces. *Applied Surface Science*, **370**, 403–409.

Heller-Kallai L. & Lapides I. (2007) Reactions of kaolinites and metakaolinites with NaOH-comparison of different samples (Part 1). *Applied Clay Science*, **35**, 99–107.

Hensen E.J.M., Poduval D.G., Degirmenci V., Ligthart D.A.J.M., Chen W., Rigutto M.S. & Veen J.A.R. Van. (2012) Acidity Characterization of Amorphous Silica – Alumina. *The Journal of Physical Chemistry C*, **116**, 21416–21429.

Johnson E.B.G. & Arshad S.E. (2014) Hydrothermally synthesized zeolites based on kaolinite: A review. *Applied Clay Science*, **97–98**, 215–221.

Kumar S., Panda A.K. & Singh R.K. (2013) Preparation and characterization of acids and alkali treated kaolin clay. *Bulletin of Chemical Reaction Engineering and Catalysis*, **8**, 61–69.

Lee S., Kim Y.J. & Moon H.S. (1999) Phase transformation sequence from kaolinite to mullite investigated by an energy-filtering transmission electron microscope. *Journal of the American Ceramic Society*, **82**, 2841–2848.

Leonard A.J. (1977) Structural Analysis of the Transition Phases in the Kaolinite-Mullite Thermal Sequence. *Journal of the American Ceramic Society*, **60**, 37–43.

Li N., Li T., Liu H., Yue Y. & Bao X. (2017) A novel approach to synthesize in-situ crystallized zeolite/kaolin composites with high zeolite content. *Applied Clay Science*, **144**, 150–156.

Lin L., Chao K., Ling Y., Hwang J. & Hou L. (1997) Characterization of the Effects of Vanadium Traps in Cracking Catalysts by Imaging Secondary Ion Mass Spectrometry and Microactivity Test. *Journal of Chinese Chemical Society*, **44**, 553–558.

Liu H., Zhao H., Gao X. & Ma J. (2007) A novel FCC catalyst synthesized via in situ overgrowth of NaY zeolite on kaolin microspheres for maximizing propylene yield. *Catalysis Today*, **125**, 163–168.

Liu X., Yan Z., Wang H. & Luo Y. (2003) In-situ synthesis of NaY zeolite with coal-based kaolin. *Journal of Natural Gas Chemistry*, **12**, 63–70.

Liu X., Liu X. & Hu Y. (2015) Investigation of the thermal behaviour and decomposition kinetics of kaolinite. *Clay Minerals*, **50**, 199–209.

Low I.M. & McPherson R.R. (1988) The structure and composition of Al-Si spinel. *Journal of Materials Science Letters*, **7**, 1196–1198.

Lutz W. (2014) Zeolite Y: Synthesis, Modification, and properties – a case revisited. *Advances in Materials Science and Engineering*, **2014**, 1–20.

Mackenzie K.J.D. & Smith M.E. (2013) *Multinuclear Solid-State NMR of Inorganic Materials*. Pergamon Materials Series. Pergamon Press, Oxford, UK, 748 pp.

Madani A., Aznar A., Sanz J. & Serratosa J.M. (1990) ^{29}Si and ^{27}Al NMR study of zeolite formation from alkali-leached kaolinites. Influence of thermal preactivation. *Journal of Physical Chemistry*, **94**, 760–765.

Magee J.S. & Mitchell M.M.J. (1993) *Fluid Catalytic Cracking: Science and Technology*. Elsevier Science Publishers B.V., Amsterdam, The Netherlands.

Mägi M., Lippmaa E., Samoson A., Engelhardt G. & Grimmer A.R. (1984) Solid-state high-resolution silicon-29 chemical shifts in silicates. *Journal of Physical Chemistry*, **88**, 1518–1522.

Man P.P., Peltre M.J. & Barthomeuf D. (1990) Nuclear magnetic resonance study of the dealumination of an amorphous silica-alumina catalyst. *Journal of the Chemical Society, Faraday Transactions*, **86**, 1599–1602.

Massiot D. (1995) ^{27}Al and ^{29}Si MAS NMR study of kaolinite thermal decomposition by controlled rate thermal analysis. *Journal of American Ceramic Society*, **78**, 2940–2944.

Okada K., ŌTsuka N. & Ossaka J. (1986) Characterization of spinel phase formed in the kaolin-mullite thermal sequence. *Journal of the American Ceramic Society*, **69**, C-251-C-253.

Pan S.S., Lin L.T.X., Komvokis V., Spann A., Clough M. & Yilmaz B. (2015) Nanomaterials fueling the world. Pp. 3–18 in: *ACS Symposium Series* (J. Louise & L. Bashir, editors). American Chemical Society, Washington, DC, USA.

Patrylak L., Likhnyovskyi R., Vypyraylenko V., Leboda R. & Skubiszewska-zi J. (2001) Adsorption properties of zeolite-containing microspheres and FCC catalysts based on Ukrainian kaolin. *Adsorption Science & Technology*, **19**, 525–540.

Peng H., Vaughan J. & Vogrin J. (2018) The effect of thermal activation of kaolinite on its dissolution and re-precipitation as zeolites in alkaline aluminate solution. *Applied Clay Science*, **157**, 189–197.

Pereira P.M., Ferreira B.F., Oliveira N.P., Nassar E.J., Ciuffi K.J., Vicente M.A., Trujillano R., Rives V., Gil A., Korili S. & de Faria E.H. (2018) Synthesis of zeolite A from metakaolin and its application in the adsorption of cationic dyes. *Applied Sciences*, **8**, 608.

Plançon A., Giese R.F. & Snyder R. (1988) The Hinckley Index for kaolinites. *Clay Minerals*, **23**, 249–260.

Ptáček P., Frajkorová F., Šoukal F. & Opravil T. (2014) Kinetics and mechanism of three stages of thermal transformation of kaolinite to metakaolinite. *Powder Technology*, **264**, 439–445.

Qiang L., Ying Z., Zhijun C., Wei G. & Lishan C. (2010) Influence of synthesis parameters on the crystallinity and Si/Al ratio of NaY zeolite synthesized from kaolin. *Petroleum Science*, 403–409.

Rocha J. & Klinowski J. (1990) Solid-State NMR Studies of the Structure and Reactivity of Metakaolinite. *Angewandte Chemie International Edition in English*, **29**, 553–554.

Rouquerol F., Rouquerol J. & K., S. (1998) *Adsorption by Powders & Porous Solids: Principios, Methodology and Applications*. Academic Press, London, UK, 485 pp.

Sadeghbeigi R. (2012) *Fluid Catalytic Cracking Handbook: An Expert Guide to the Practical Operation, Design, and Optimization of FCC Units*, 3rd edn. Butterworth Heinemann, Oxford, UK, 352 pp.

Salagre P., Fierro J.L.G., Medina F. & Sueiras J.E. (1996) Characterization of nickel species on several γ-alumina supported nickel samples. *Journal of Molecular Catalysis A: Chemical*, **106**, 125–134.

Sonuparlak B., Sarikaya M. & Aksay I.A. (1987) Spinel phase formation during the 980°C exothermic reaction in the kaolinite-to-mullite reaction series. *Journal of the American Ceramic Society*, **70**, 837–842.

Sousa-Aguiar E.F., Trigueiro F.E. & Zotin F.M.Z. (2013) The role of rare earth elements in zeolites and cracking catalysts. *Catalysis Today*, **218–219**, 115–122.

Sperinck S., Raiteri P., Marks N. & Wright K. (2011) Dehydroxylation of kaolinite to metakaolin—a molecular dynamics study. *Journal of Materials Chemistry*, **21**, 2118–2125.

Wang H., Li C. & Peng Z. (2011) Characterization and thermal behavior of kaolin. *Journal of Thermal Analysis and Calorimetry*, **105**, 157–160.

Wei B., Liu H., Li T., Cao L., Fan Y. & Bao X. (2010) Natural rectorite mineral: a promising substitute of kaolin for *in situ* synthesis of fluid catalytic cracking catalyst. *American Institute of Chemical Engineers Journal*, **56**, 2913–2922.

Woltermann G.M., Magee J.S. & Griffith S.D. (1993) Fluid catalytic cracking: science and technology. Pp. 105–144 in: *Studies in Surface Science and Catalysis* (J.S. Magee & M.M.J. Mitchell, editors). Elsevier Science Publishers B.V., Amsterdam, The Netherlands.

Xu M., Cheng M. & Bao X. (2000) Growth of ultrafine zeolite Y crystals on metakaolin microspheres. *Chemical Communication*, 1873–1874.

Zhang Y. & Xiong C. (2012a) A new way to enhance the porosity and Y-faujasite percentage of in situ crystallized FCC catalyst-Supplement info. *Catalysis Science & Technology*, **2**, 606–612.

Zhang Y. & Xiong C. (2012b) A new way to enhance the porosity and Y-faujasite percentage of in situ crystallized FCC catalyst. *Catalysis Science & Technology*, **2**, 606–612.

Zheng S.-Q., He L.-J., Ren S., Yu H.-X. & Zhu W. (2015) A novel FCC catalyst based on a porous composite material synthesized via an in situ technique. *Kemija u industriji*, **64**, 603–610.

Zheng S., Sun S., Zhang Z., Gao X. & Xu X. (2005a) Effect of properties of calcined microspheres of kaolin on the formation of NaY zeolite. *Bulletin of the Catalysis Society of India*, **4**, 12–17.

Zheng S., Sun S., Wang Z., Gao X. & Xu X. (2005b) Suzhou kaolin as a FCC catalyst. *Clay minerals*, **40**, 303–310.

https://doi.org/10.1180/clm.2020.40 Published online by Cambridge University Press